SPACE RADIATION ENVIRONMENT

Henry B. Garrett
Jet Propulsion Laboratory, California Institute of Technology,
4800 Oak Grove Dr., Pasadena, CA 91109 USA

Abstract

Coupled with the increasing concern over trapped radiation effects on microelectronics, the availability of new data, long term changes in the Earth's magnetic field, and observed variations in the trapped radiation fluxes have generated the need for better, more comprehensive tools for modeling and predicting the Earth's trapped radiation environment and its effects on space systems. The objective of this report is to describe the current status of those efforts and review methods for attacking the issues associated with modeling the trapped radiation environment in a systematic, practical fashion. The ultimate goal will be to point the way to increasingly better methods of testing, designing, and flying reliable microelectronic systems in the Earth's radiation environment. The review will include a description of the principle models of the trapped radiation environment currently available--the AE8 and AP8 models. Recent results from radiation experiments on spacecraft such as CRRES, SAMPEX, and CLEMENTINE will then be described.

1. The Trapped Radiation Environment

By definition, the high energy particle radiation environment in space consists of electrons with energies greater than 40 KeV, protons or neutrons with energies greater than 1 MeV, and heavy ions with energies above 1 MeV/nucleon. Lower energy electrons and protons, and ions are ubiquitous, but are considered as plasma. The populations are characterized in terms of their kinetic energy, charge state, and composition. Unlike photons which travel uniformly at the speed of light, particles can vary in velocity from a few m/s up to a sizable fraction of the speed of light in the case of cosmic rays. The high energy radiation population can be roughly divided into four families based on these characteristics:

1) Galactic Cosmic Rays (interplanetary protons, electrons, and ionized heavy nuclei);
2) Trapped radiation (for the Earth, the Van Allen Belts);
3) Protons and other heavy nuclei associated with solar proton events.
4) Neutrons (primarily Cosmic Ray Albedo Neutrons or CRAN particles).

Each type of radiation has a characteristic spectrum and preferred interaction mode with matter that supports this simple division. Here the discussion will focus primarily on the trapped radiation environment, the Van Allen Belts. First discovered by J. Van Allen and his collaborators on Explorer I, trapped radiation at the Earth consists principally of energetic protons and electrons, with lesser percentages of heavy ions such as O^+, contained in toroidal belts by the Earth's magnetic field. This toroid is commonly known as the "Van Allen belt(s)"[1] and consists of (at least) two zones: a low altitude zone, or "inner belt"; and a high altitude zone, or "outer belt". The inner belt extends from ~100s of km to ~ 6,000 km in altitude and is populated by high-energy (~10s of MeV) protons and medium energy (50-1000 keV) electrons, while the outer belt, up to 60,000 km in altitude, is predominately high energy electrons. Schematics of the radiation flux contours for the Van Allen belts are illustrated in Fig. 1[2]. The detailed mechanism by which particles are entrapped in the belt regions is not well understood nor is the primary source clearly identified–observations of abundance ratios imply both terrestrial and interplanetary sources. Once captured, the motion of charged particles in the Earth's magnetic field is governed by the Lorentz force. The trapped radiation environment also exhibits large temporal variations. The inner belt zone, because of the dominance of the Earth's main field, is relatively stable. Most temporal variations in this population occur as the solar cycle proceeds and the Earth's neutral atmospheric density at a given altitude changes causing variations in the altitude at which radiation particles can mirror without being scattered. Variations of an order of magnitude over a period of months have been observed in the electron flux intensities[3] as a result of extended elevated geomagnetic activity. In contrast, the outer belt, which is more influenced by the Earth's highly variable

geomagnetic tail, experiences much greater temporal fluctuations. The electron concentration in the outer zone may experience temporal fluctuations as large as a factor of 100,000. Fortunately, most of the physical damage caused by the trapped radiation is largely attributable to the long-term cumulative (or integral) dose received by the spacecraft rather than the instantaneous fluctuations of the radiation.

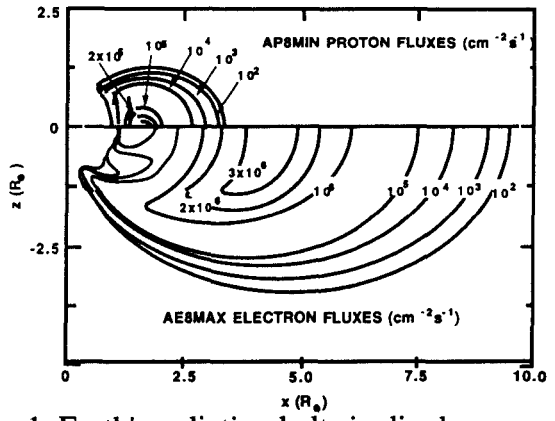

Fig. 1. Earth's radiation belts in dipole space, according to the AP8 and AE8 models. Average omnidirectional integral fluxes above energy thresholds are shown.[2]

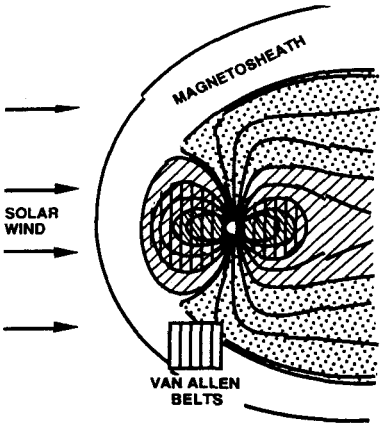

Fig 2. Cross section of Earth's magnetic field in noon-midnight meridian showing structure of field lines and overlapping plasma regions.

2. Geomagnetic Field

The major factor in the control of the radiation belts is the geomagnetic field. Aside from the gravitational field of the Earth, the geomagnetic field due to the internal geomagnetic field is the most accurately known of the natural environments. It can be crudely modeled in terms of a tilted (-11° from geographic north) magnetic dipole of magnitude $M = 8 \times 10^{25}$ G-cm^3 (G is the magnetic unit Gauss). Ignoring the tilt for the moment, in the geomagnetic coordinate system, the magnetic field intensity induced by M at the point (r,θ,ϕ) is given by the expression:

$$B_i = -(M/r^3) \cdot (3\cos(\theta) + 1)^{0.5} \qquad (1)$$

In the Gaussian unit system, r is in cm, and B_i is in G. Given the above value for M, B_i is then found to have a maximum value of ~0.6 G near the polar cap and a minimum value of ~0.3 G near the equator at the Earth's surface. Eq. 8 is valid only for an idealized configuration of a centered dipole. In reality, large scale discrepancies (as high as ±25%) exist between the measured data and the ideal, dipole expression. For most purposes, the IGRF series of models is the official standard. Fig. 2 is a cross section of the Earth's magnetic field in the noon-midnight meridian. There are two minima near the equator--the largest of these is responsible for the so-called South Atlantic Anomaly, a region critical in determining radiation exposure in LEO.

3. AE8 and AP8 Models

The AP8/AE8 models are currently the principle source of data on the trapped radiation environment. They are based on compiled data from many different satellites.[4-6] The P and E in the model names AP8 and AE8 refer to "Proton" and "Electron" and 8 is the version number of the models. AP8 and AE8 provide estimates of the omnidirectional fluxes of protons in the energy range of ~50 keV to 500 MeV and electrons in the energy range of ~50 keV to ~7 MeV. Time-dependent variations of the radiation fluxes such as those due to geomagnetic storms or short term solar modulations are not included in AP8/AE8. However, the models do differentiate between solar cycle maximum and minimum conditions. The AE/AP model fluxes are parametrically represented by:

$$I(>E,B,L,\tau,T) = N(>E,L)\Phi(>E,L,\tau)G(B,L) \qquad (2)$$

where I is the integral omnidirectional flux, >E means for all energies above E, τ is the local time, T is the epoch (or date), and L is the McIlwain L coordinate. Data from many different satellites are averaged in discrete B and L bins to determine the B-L variation G; in energy, L, and local time to

determine the local time variation Φ; and in energy and L bins to determine the energy variations N. As discussed by Vette and his collaborators, there are unfortunately many regions of spotty spatial coverage[4].

For comparison with data, Figure 3 illustrates approximately one year's worth of hourly averages of the 1.9 MeV omnidirectional electron flux measured at midnight by the geosynchronous satellite ATS 1[7]. The daily sum of the geomagnetic index K_p (at the bottom of the figure) and the value predicted by the AE model (the horizontal line) are also plotted. This figure demonstrates two important points. First, the electron radiation flux at L=6.6 is highly variable on a daily time scale--some variations being on the order of 10 to 100.

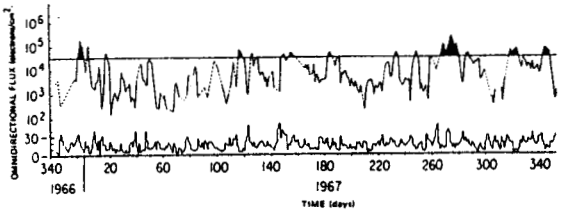

Fig. 3. Hourly averages of ATS 1 1.9 MeV omnidirectional e⁻ flux at midnight.[7] Daily sum of K_p at bottom of figure. Horizontal line is AE model equatorial flux at L = 6.6 at midnight.

Secondly, the AE model is biased toward the few major geomagnetic storms. This biasing is to be expected as the model is derived by averaging fluxes. Errors in estimating the radiation environment can have substantial economic impact through excessive shielding mass or early satellite loss. Vampola[8] has attempted such estimates and finds the models to be within a factor of 2 for long time averages (for 5 to 10 year averages) of the observed results.

4. CRRES Models

Given the many known uncertainties in the AE/AP models, the DoD (primarily the Air Force Phillips Laboratory) and NASA developed the CRRES satellite program. CRRES was launched on July 25, 1990 (it ceased transmitting on 12 October 1991) and was placed in a 18.1°, 350 km by 33,000 km orbit with a period of 10 hours. The satellite carried a complete complement of radiation environment sensors and was in an ideal orbit for mapping the trapped radiation belts. Approximately 14 months of data during Solar Maximum were obtained before a battery failure terminated the mission. The data have been used to develop several new models of the trapped radiation environment and to test the AE/AP models[9-11]. Two trapped radiation models based on the CRRES data have been developed (CRRESRAD[9] and a model of outer zone electrons[10]).

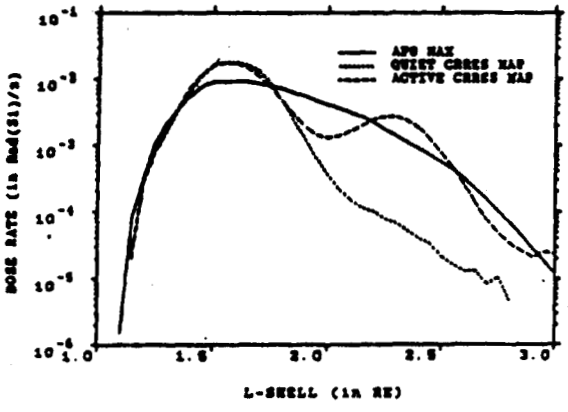

Fig. 4. Dose rate along magnetic equator as a function of L for quiet and active CRRES dose models and for AP8MAX. Dose rate for E>20 MeV protons.[11]

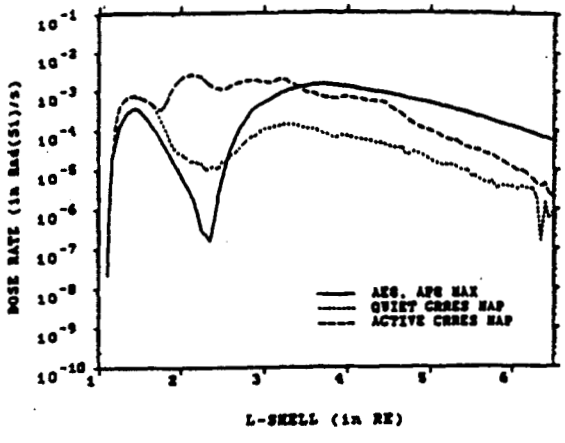

Fig. 5. Dose rate at magnetic equator as function of L for quiet/active CRRESRAD and for AP8MAX/AE8MAX. Dose rate is for E>2.5 MeV electrons and E>135 MeV protons.[11]

The CRRESRAD model[9] is a PC-based software program that provides estimates of the dose behind four shielding thicknesses for a large range of satellite orbits. The model is based on the Space Dosimeter experiment[12] which returns dose data in the energy ranges 50 keV to 1 MeV (LOLET) and 1 to 10 MeV (HILET). The dose is measured behind four thicknesses of hemispherical aluminum shielding (0.57, 1.59, 3.14, and 6.08 gm/cm^2). These correspond to electrons with energy greater than 1, 2.5, 5, and 10 MeV and protons with energy greater than 20, 35, 52, and 75 MeV. Sample data for the CRRESRAD model are plotted in Figs. 27 and 28[11]. These results are for the dose rate, in Rad(Si)/s, as a function of L along the magnetic equator. The data are plotted in terms of HILET (for protons > 20 MeV) and LOLET (>2.5 MeV electrons and >135 MeV protons) for the quiet and active models and for the AE8 and AP8 models. The figures illustrate the differences between the CRRES and AE/AP models. Specifically, in Figure 27, there is relative agreement between the active CRRES model and the AP8 model for E>20 MeV protons whereas the low activity CRRES model is about an order of magnitude lower in dosage for L>2. At higher energy cutoffs, this difference is reversed with the AP8 model agreeing more closely with the quiet model and being an order of magnitude lower than the active model for L>2. These differences are explainable in terms of a second, variable proton belt extending between L=1.8-4 present in the CRRES active model that is not present in the AE/AP models. For Fig. 28, there are much larger differences between the models. In particular, the AE/AP model results exceed the CRRES models for L>3.5 (primarily because of the >2.5 MeV electrons) and is lower for L<2.5. There are in fact differences of three orders of magnitude between the active model and 1.5 orders between the quiet model and the AE/AP model in the so-called slot region near L=2.5. There are other differences between the models, but these figures illustrate the major concerns--namely the extra proton belt in the CRRES active data and the lack of high energy electrons in the NASA models.

5. Magnetospheric Heavy Ions

Grigorov et al.[13] and Cummings et al.[14] have presented evidence for an energetic ($\geq$15 MeV/nuc) trapped heavy ion component associated with the Galactic Cosmic Ray (GCR) anomalous component. Blake and Friesen[15] suggested that the anomalous cosmic ray (ACR) component particles, which may be only singly ionized initially, can penetrate deeper into the magnetosphere than the normal GCR component which is typically fully ionized. The particles are then ionized near their geomagnetic cutoff and become trapped. This leads to a special trapped population of oxygen, nitrogen, neon, and other elements which may be the source of the observed heavy ion component. The SAMPEX spacecraft[14] has observed $\geq$15 MeV/nuc trapped heavy ions with Z$\geq$2. The trapped population includes He, N, O, and Ne and is located at L~2.[14]

The population was seen to increase in intensity in concert with a similar increase in the ACR component. The geographic distribution of the oxygen particles detected by SAMPEX (which is in an 82° inclination orbit with an apogee of ~670 km and a perigee of ~520 km) is illustrated in Fig. 6. The SAMPEX observations verify that the ACR mechanism predicted by Blake and Friesen is a source of trapped ions N, O, and Ne above 27, 21, and 14 MeV/nuc. Helium ions were also observed but this population is believed to have been trapped by another mechanism than that proposed by Blake and Friesen and may have another source.[14]

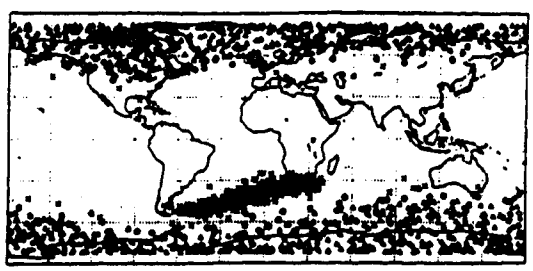

Fig. 6. Distribution of oxygen ions observed by SAMPEX between 1992 and 1993.[14] Triangles: events with cutoff energy above vertical O^{+6}; crosses: events with cutoff energy less than $O^{+1.5}$; and circles: events with intermediate cutoff energy.

6. Estimating Radiation Effects On Parts And Materials

The primary practical reason for interest in the trapped radiation environment is its effects on microelectronics. Microelectronic parts testing, characterization, and selection are potentially

among the most expensive and time consuming processes in spacecraft design. For radiation interactions with parts, 3 "particle" families need to be considered: photons (primarily EUV, X-ray, and γ-rays); charged particles (protons, electrons, and heavy ions); and neutrons. Mass, charge, and kinetic energy are the principle physical characteristics of interest whereas mass and density are the key characteristics for the target material. Here the types of interactions will be discussed in terms of the first two particle families (neutrons will be ignored as they play no role in the effects of trapped radiation belts on spacecraft systems). The effects of the shielding on these particles are manifested in terms of energy deposited in a volume (dose) or energy deposited per unit length in the target material (LET) after traversing the shielding. The radiation shielding calculation necessary to determine the environment inside a spacecraft breaks down into a 3 step process for each particle: 1) Definition of the ambient environment; 2) Propagation of that environment through the shield and calculation of the subsequent changes in the spectrum up to the target; and 3) Estimation of the total energy and/or the energy deposition rate at the target.

6.1 Particle Interactions

Photons, which propagate at the speed of light and have no charge or rest mass, interact primarily through the photoelectric effect, Compton scattering, and pair production. These interactions all generate free electrons. In the photoelectron process, the photon is completely absorbed by the emitted (typically) outer shell electron. In one case, however, subsequent interactions are possible—that is, if the photon is energetic enough to emit K-shell electrons (inner shell electrons), then this process will dominate ~80% of the time over the emission of outer shell electrons. When an L-shell (or outer shell) electron subsequently drops down to fill the K-shell vacancy, it can emit either an additional X-ray or a low energy Auger electron from the L-shell (dependent on the Z of the material). In Compton scattering, the incident photon is not completely absorbed as the photon is of much greater energy than the atomic electron binding energy. Part of the photon energy goes to scattering the atomic electron (called a Compton electron) and the rest into a scattered, lower energy photon. Pair production takes place for photons at energies of 1.02 MeV or higher. A photon of this energy will be completely absorbed by a high-Z material. A positron-electron pair will then be formed. Figure 7[16] compares the ranges over which each of the 3 interactions dominate as functions of Z and energy. For reference, in silicon, the photoelectron effect dominates at energies <50 keV, pair production for energies >20 MeV, and Compton scattering at intermediate energies.

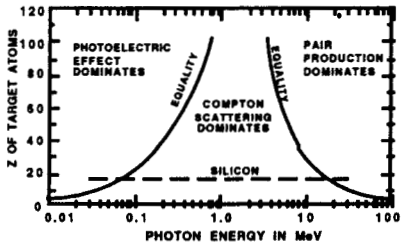

Fig. 7. Importance of photon interactions versus Z and energy. Solid lines correspond to equal interaction cross sections for neighboring effects. Dashed line is for photon interactions with silicon.[16]

Charged particles interact with matter primarily in 2 ways: Rutherford scattering and nuclear interactions. Rutherford (or Coulomb) scattering, in which the charged particle interacts with the electric field of the target atom, typically dominates. It results in both excitation and ionization of atomic electrons and can, for sufficiently energetic impacts, transfer enough energy to displace atoms within the lattice structure. As an example, for electrons, a minimum energy of ~150 KeV is required to cause displacement in silicon while only 100 eV is required for protons. Nuclear interactions, where the impacting particle actually interacts with the atomic nucleus, can result in elastic or inelastic scattering and transmutation (through fusion or fission). As an example, a nucleus can absorb a proton and emit an alpha particle. This process, also called spallation, and the recoil atoms that result from displacement can transform a relatively benign proton environment into a SEU-causing heavy ion environment as the heavy ions have much larger LETs compared with the protons. Also, long term exposure to the space radiation environment can, through transmutation, lead to making the spacecraft material itself radioactive.

One quantitative measure of the interaction of a high energy particle with matter is stopping power or energy loss per unit length in a given material. As an example, low energy electrons (~10 KeV) primarily cause ionization. The amount of energy deposited by the latter and protons in producing ionization can be determined from stopping power tables (electrons: Berger and Seltzer[17]; protons: Janni[18, 19]). Stopping power is essential in calculating the Heinrich flux necessary for most SEU calculations. Stopping power (or, approximately, LET) in terms of MeV-cm^2/g is given in Fig. 8 for electrons, protons, and various heavy ions in silicon.[20]

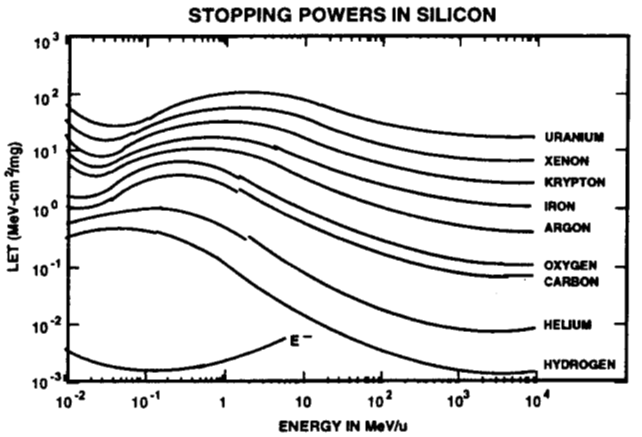

Fig. 8. The stopping power (or LET) in MeV-cm^2/g versus energy per atomic mass unit for a variety of ions (MeV/μ) and electrons (MeV) in silicon.[20]

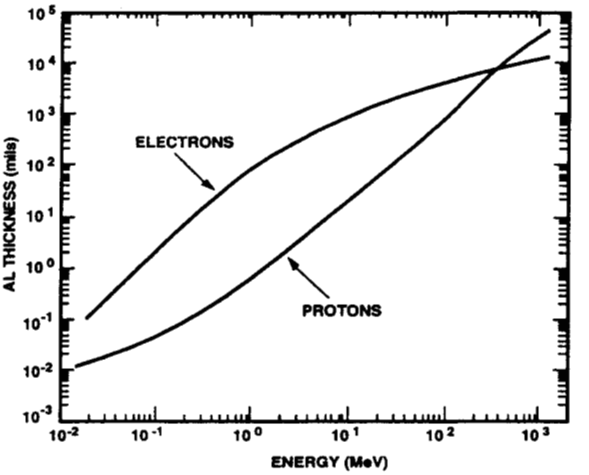

Fig. 9. Minimum penetration energy for electrons and protons versus shield thickness.

A second quantitative measure of high energy particle interactions closely related to stopping power is the penetration depth/range or maximum distance a particle of a given energy can penetrate. This depth can be used to estimate the cut-off energy for a given thickness of spacecraft shielding and hence its effectiveness. Fig. 9 compares the penetration depth of electrons and protons in aluminum for different energies. Note that a 1 MeV electron penetrates ~100 times more shielding (~0.2 cm) than a 1 MeV proton (~0.0015 cm). Similarly, it takes a ~20 MeV proton to penetrate the same depth as a 1 MeV electron. As ~0.1-0.2 cm (40–80 mils) is a typical shielding level, it is common to compare the integral dose for $E \geq 1$ MeV electrons with $E \geq 20$ MeV protons as these are the primary contributors to the radiation environment behind the spacecraft shield.

6.2 Modeling The Effects Of Shielding

If the detailed evolution of a particle passing through matter is followed, the interaction of the particle with shielding becomes increasingly complex as each interaction gives rise to a cascade of by-products. Fortunately, a point is reached where the by-products and the original incident particle (if it still exists) no longer have sufficient energy to excite further interactions—the process has a finite conclusion. It is common practice to use Monte Carlo techniques to model the detailed passage of a particle through shielding and to estimate the end products of the multiple particle interactions that are created following a single particle impact. The effects of the by-products are then approximated roughly in terms of displacement damage, energy deposition, or ionization (or electron-hole creation).

Electrons are particularly easily scattered in a material. This behavior is illustrated in Fig. 11 which is a computer simulation (Monte Carlo) of the trajectories of electrons impacting on an "infinitely thick" copper target[21, 22]—note that many of the electrons are actually scattered back out of the surface of the material. It is readily apparent in these Monte Carlo simulations that the dose is dependent on the shape (or thickness) of the shield. This scattering of the electrons and their by-products by the shielding means that the details of geometry of the shielding must be considered in any radiation calculations.

As an illustration of the process of estimating the radiation dose environment within a satellite, consider the trapped radiation environment anticipated by the CLEMENTINE interstage satellite. Assuming a spherical shell shield, the dosages expected for the CLEMENTINE interstage mission are summarized in Fig. 12 (the interstage had a perigee of ~500 km, an apogee of ~160,000 km, and an inclination of 67°). Note that the proton dose due to trapped radiation is very low in comparison to the trapped electrons for the interstage. Fig. 12 is representative of the type of design information usually provided to a project for estimating effects on electronic components.

Fig. 11. Computer plot of electron trajectories in Cu target for 20 keV beam normal to surface.[21, 22]

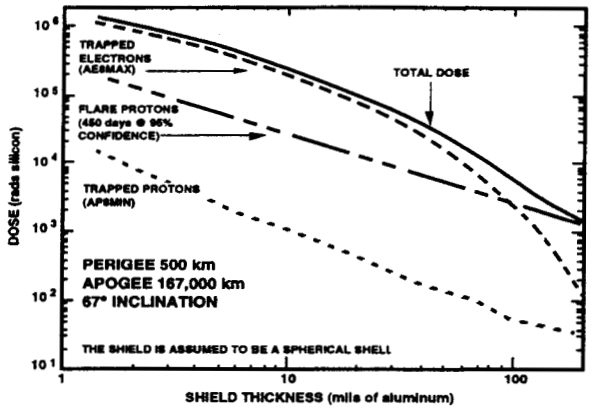

Fig. 12. CLEMENTINE Interstage mission total dose-assumes 450 day mission and 95% confidence flare environment (spherical aluminum shield configuration).

7. Conclusion

The objective of this report was to address 3 aspects of the radiation problem. First, a review was provided of the natural and man-made space radiation environments. Secondly, the methods used to propagate the external environment through the complex spacecraft structures surrounding the point where the internal radiation environment was required were discussed. An example of the environment inside a spacecraft was then presented. While not intended to treat in detail all aspects of the problem of the radiation environment within a spacecraft, it is hoped that a basis for understanding the process of predicting the internal spacecraft radiation environment has been established.

Acknowledgments

The research in this paper was carried out by the Jet Propulsion Laboratory, California Institute of Technology under contract with the National Aeronautics and Space Administration.

References

[1] J. A. Van Allen, *Geomagnetically Trapped Radiation*, Space Science, J. Wiley & Sons, Inc., New York-London, (1963).

[2] E. J. Daly, "The Evaluation of Space Radiation Environments for ESA Projects," *ESA Journal*, Vol. 12, pp. 229-247 (1988).

[3] A. L. Vampola, "Effects of the March-June Magnetic Storm Period on Magnetospheric Electrons," *Solar-Terrestrial Predictions-IV, Proceedings of a Workshop at Ottawa, Canada, May 18-22, 1992*, Ottawa, Canada, NOAA/SEL, Boulder, CO, (1993).

[4] J. I. Vette, M. J. Teague, D. M. Sawyer and K. W. Chan, "Modeling the Earth's Radiation Belts," *Solar-Terrestrial Prediction Proceedings*, Boulder, NOAA, (1979).

[5] D. M. Sawyer and J. I. Vette, "AP-8 Trapped Proton Environment for Solar Maximum and Solar Minimum," 76-06, NSSDC/WDC-A-R&S (1976).

[6] J. I. Vette, "The AE-8 Trapped Electron Model Environment," 91-24, NSSDC/WDC-A-R&S (1991).

[7] K. Chan, M. J. Teague, N. Schofield and J. I. Vette, "Modeling of electron time variations in the radiation belts," in *Quantitative Modeling of Magnetospheric Processes,* W. P. Olson, Editor American Geophysical Union, Washington, D.C., pp. 121 (1979).
[8] A. L. Vampola, "Radiation effects on space systems and their modeling," in *Space Systems and Their Interactions with Earth's Space Environment,* H. B. Garrett and C. P. Pike, Editors, AIAA, New York, pp. 339 (1980).
[9] K. J. Kerns Capt., USAF and M. S. Gussenhoven, "CRRESRAD Documentation," PL-TR-92-2201, Phillips Laboratory Directorate of Geophysics (1992).
[10] D. H. Brautigam, M. S. Gussenhoven and E. G. Mullen, "Quasi-Static Model of Outer one Electrons," *submitted to IEEE Trans. Nucl. Sci.*, No. December, (1992).
[11] M. S. Gussenhoven, E. G. Mullen and D. H. Brautigam, "Near-Earth Radiation Model Deficiencies as seen on CRRES," *COSPAR 1993*, (1993).
[12] D. A. Hardy, F. Hanser and B. Sellers, "The Space Radiation Dosimeter (AFGL-701-2)," in *CRRES/SPACERAD Experiment Descriptions,* M. S. Gussenhoven, E. G. Mullen and R. C. Sagalyn, Editors, AF Geophysics Laboratory, Hanscom AFB, MA, (1985).
[13] N. L. Grigorov and e. al., "Evidence for Anomalous Cosmic Ray Oxygen Ions in the Inner Magnetosphere," *Geo. Res. Ltrs.*, Vol. 18, pp. 1959 (1991).
[14] J. R. Cummings, A. C. Cummings, R. A. Mewaldt, R. S. Selesnick, E. C. Stone and T. T. von Rosenvinge, "New Evidence for Geomagnetically Trapped Anomalous Cosmic Rays," *Geo. Res. Ltrs.*, Vol. 20, No. 18, pp. 2003-2006 (1993).
[15] J. B. Blake and L. M. Friesen, "A Technique to Determine the Charge State of the Anomalous Low Energy Cosmic Rays," *15th International Cosmic Ray Conf.*, Plovdiv, Vol. 2 (1977).
[16] P. S. Winokur, "Total-Dose Radiation Effects (From the Perspective of the Experimentalist)," *IEEE Nuc. and Space Rad. Effects Conf. Short Course*, New Orleans, LA, IEEE, II (1992).
[17] M. J. Berger and S. M. Seltzer, "Penetration of Electrons and Associated Bremsstrahlung through Aluminum Targets," SP-169, pp. 285-322, NASA, Washington, DC (1968).
[18] J. F. Janni, "Proton Range-Energy Tables, 1 keV-10 GeV, Part 1," Atomic Data and Nuclear Data Tables, pp. 150-339 (1982).
[19] J. F. Janni, "Proton Range-Energy Tables, 1 keV-10 GeV, Part 2," Atomic Data and Nuclear Data Tables, pp. 341-529 (1982).
[20] J. H. Adams Jr., "Cosmic Ray Effects on Microelectronics, Part IV," NRL Memorandum Report 5901, Naval Research Laboratory, Washington D.C. (1986).
[21] L. Curgenven and P. Duncumb, "Report 303," Tube Investments Research Laboratories (1971).
[22] D. B. Brown, "Total Dose Effects at Dose Rates Typical of Space," *NSREC Short Course*, IEEE NSREC, (1990).